Optics and Laser Technology 101 (2018) 138–143

Contents lists available at ScienceDirect

Optics and Laser Technology

journal homepage: www.elsevier.com/locate/optlastec

Full length article

All-optical analog-to-digital converter based on Kerr effect in photonic crystal

Dariush Jafari [a], Tofiq Nurmohammadi [c], Mohammad Javad Asadi [d], Karim Abbasian [a,b,*]

[a] School of Engineering Emerging Technologies, University of Tabriz, Tabriz 51666, Iran
[b] Electrical Engineering Department, University of Bonab, Bonab 55517, Iran
[c] Faculty of Electrical and Computer Engineering, University of Tabriz, Tabriz 51664, Iran
[d] Lehigh University, Bethlehem, PA 18015, USA

ARTICLE INFO

Article history:
Received 29 May 2017
Received in revised form 26 September 2017
Accepted 4 November 2017

Keywords:
Nonlinear material
Photonic crystal (PhC)
Finite difference time domain (FDTD) method
All-optical analog-to-digital converter (AOADC)

ABSTRACT

In this paper, a novel all-optical analog-to-digital converter (AOADC) is proposed and simulated for proof of principle. This AOADC is designed to operate in the range of telecom wavelength (1550 nm). A cavity made of nonlinear Kerr material in photonic crystal (PhC), is designed to achieve an optical analog-to-digital conversion with 1 Tera sample per second (TS/s) and the total footprint of 42 μm^2. The simulation is done using finite-difference time domain (FDTD) method.

1. Introduction

Electronic-to-optical conversion and vice versa in integrated optical circuits and networks reduce the bandwidth and limit the speed of operation. One of the best solution proposed is to take advantage of all-optical devices. In recent years, all-optical devices, such as switches [1–3], logic gates [2,4–6], add-drop filters [7,8], and multiplexers [9,10]. based on photonic crystal (PhC) structures have been designed and proposed with appropriate dimensions. Nowadays, in modern communication systems, AOADCs in all-optical networks and processors can lead to increase of speed and bandwidth due to elimination of electronic conversion. However, AOADCs suffer from some limitations that hinder them to be developed commercially. For example, The first generation AOADC was designed based on a hundred-kilometer optical fiber which was not possible to be considered in all-optical integrated circuits [11,12]. Another structures was designed based on Chalcogenide in which although a significant improvement was achieved comparing the former mentioned structure, the dimension still is too large (six centimeters) to be an appropriate candidate for optical integrated circuits [13]. There are various designs for AODCs using PhCs; but operation speed of these devices is not acceptable for ultra-high-speed optical processing [14–16]. In this paper, an AOADC with tiny dimensions and maximum sampling rate up to 1 TS/s is proposed based on nonlinear Kerr effect in PhC. All the calculations and simulations of the designed AOADC are done based on Plane wave expansion (PWE) and finite-difference time domain (FDTD) methods, respectively. While most of the research in this area has been limited to theoretical and numerical analysis, there have also been practical implementation of photonic crystal structures [17,18]. In this work, an analytical and numerical investigation of the novel all-optical analog-to-digital converter (AOADC) is explored and AOADC mechanism is described analytically and findings verified by structure FDTD simulations. The results of this analytical and numerical investigation paves the path and set the direction towards the realization of all-optical AOADC which can find applications in communication and nanoplasmonic circuits. The paper is arranged in following way. In part 2, a defected cavity based on Kerr defect is designed and analyzed. Part 3 introduces the designed ADC based on the discussed defected cavity. Finally, the results are discussed and concluded in part 4.

* Corresponding author.
E-mail addresses: d.jafari89@ms.tabrizu.ac.ir (D. Jafari), tofiqnurmohammadi@tabrizu.ac.ir (T. Nurmohammadi), moa214@lehigh.edu (M.J. Asadi), k_abbasian@tabrizu.ac.ir (K. Abbasian).

https://doi.org/10.1016/j.optlastec.2017.11.007
0030-3992/

2. Defected cavity based to Kerr effect

In recent years, different logic gates and ADCs have been proposed based on cavity and nonlinear properties due to their high-speed performance and low-power consumption [19,20]. In this paper, PhC is designed based on air rods with radii r = 0.3a in GaAs substrate with refractive index of 3.49 at $\lambda = 1550$ nm, and the lattice constant of a = 434 nm. Removing a row of rods in the structure results in the band diagram of PhC, as shown in Fig. 1.

Removing two of the up and down rods along the deleted row as shown in Fig. 2, a cavity is created with a specific resonant frequency. Fig. 3 shows the model of the cavity of the structure. Based on temporal coupled mode theory [21] (TCMT) near the resonant modes, the waveguide transmission can be expressed by:

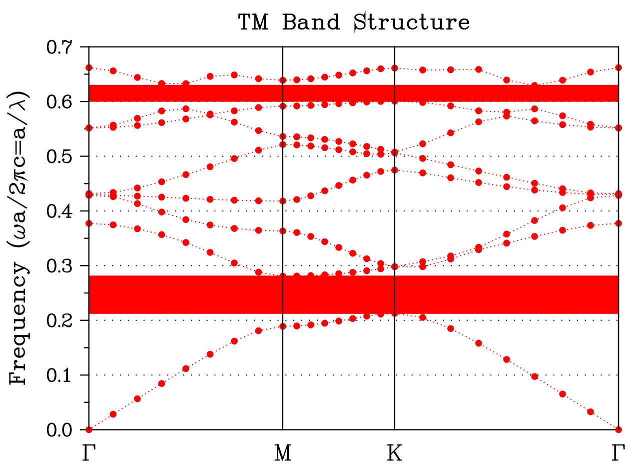

Fig. 1. The simulated band diagram of the designed PhC.

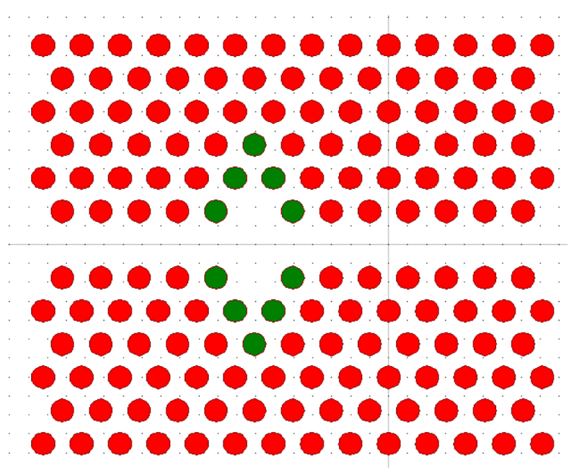

Fig. 2. Schematic of the designed PhC including removed rods and green dots creating the cavity. (For interpretation of the references to colour in this figure legend, the reader is referred to the web version of this article.)

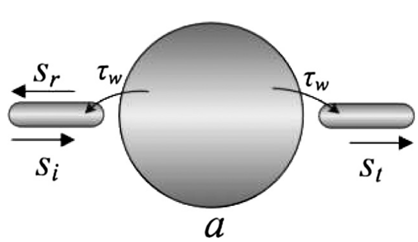

Fig. 3. Schematic of photonic crystal cavity model

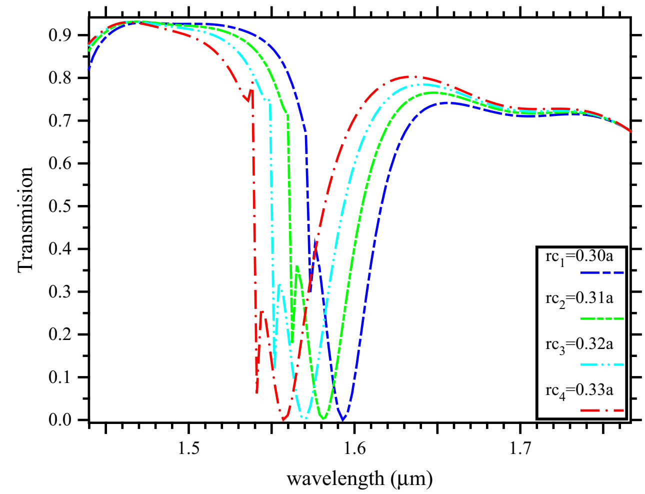

Fig. 4. Simulated transmission vs. wavelength for the PhC with the radii of the rods around the defect of $r_{C1} = 0.30a$, $r_{C2} = 0.31a$, $r_{C3} = 0.32a$, and $r_{C4} = 0.33a$.

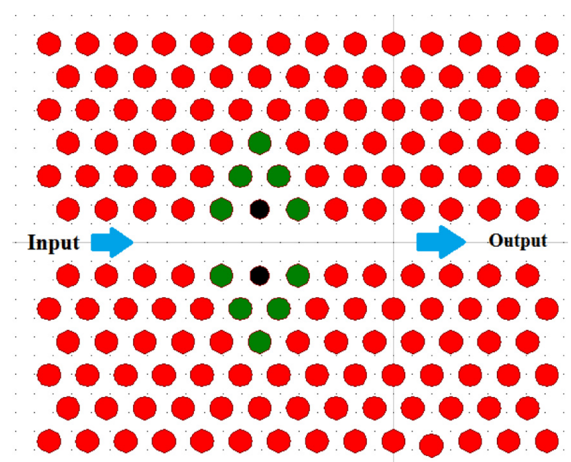

Fig. 5. Schematic of the designed PhC including the located nonlinear Kerr material (black dots) within the cavity.

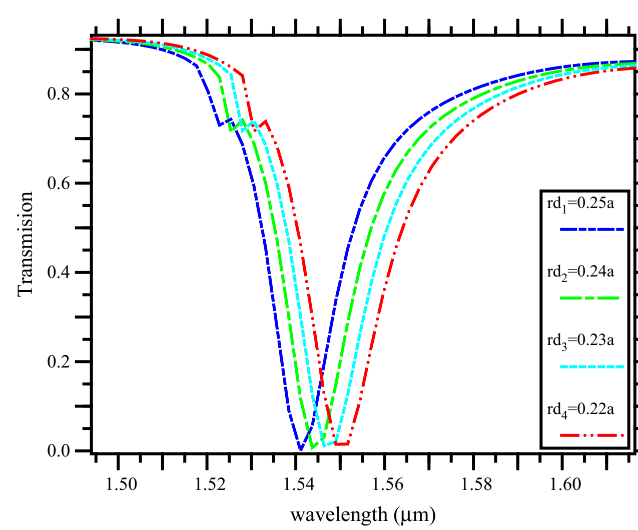

Fig. 6. Simulated transmission vs. wavelength for the PhC with the nonlinear Kerr defects with radii of $r_{d1} = 0.25a$, $r_{d2} = 0.24a$, $r_{d3} = 0.23a$ and $r_{d4} = 0.22a$.

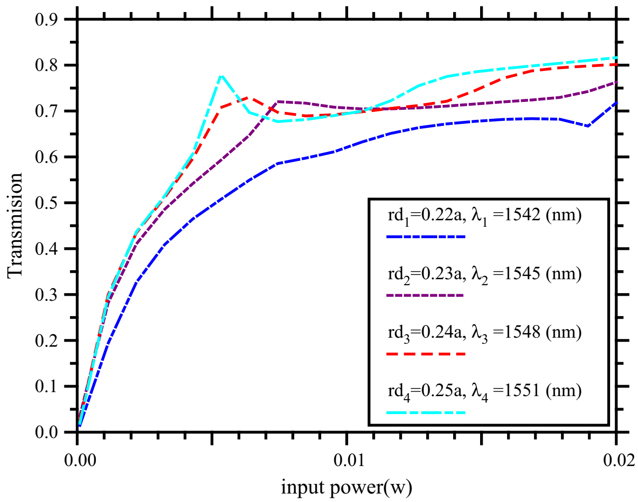

Fig. 7. Simulated transmission vs. input power for radii of $r_{d1} = 0.22a$, $r_{d2} = 0.23a$, $r_{d3} = 0.24a$, $r_{d4} = 0.25a$. at wavelength of $\lambda_1 = 1542, \lambda_2 = 1545, \lambda_3 = 1548$, and $\lambda_4 = 1551$ nm

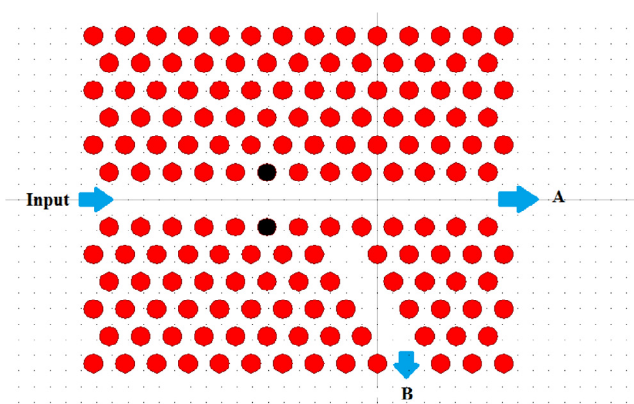

Fig. 8. The designed ADC having two output ports A and B.

$$T(\omega) = \frac{(\omega - \omega_0)^2 + \left(\frac{1}{\tau_i}\right)^2}{(\omega - \omega_0)^2 + \left(\frac{1}{\tau_i} + \frac{1}{\tau_\omega}\right)^2} \tag{1}$$

where ω stands for the frequency of incident light and ω_c is the resonance cavity frequency, $1/\tau_i$ represents the decay rate intrinsic loss, and $1/\tau_\omega$ is the waveguide coupling loss [21]. At the resonance frequency ω_0, the transmission function has a dip with a minimal value of $(1/\tau_i)^2/(1/\tau_i + 1/\tau_\omega)^2$ and Fig. 4 demonstrates transmission of the structure of Fig. 2. As Fig. 4 shows, the resonant frequency can vary by changing the radii of rods around the defects. [19,20]. Adjusting the diameters of defects, it can be possible to tune transmission dips wavelength.

As Fig. 5 illustrates, two rods with linear refractive indexes of $N_L = 2.6$ and nonlinear refractive indexes of $N_2 = 2.7e^{-9}$ m^2/W are located inside the cavity [17,18]. Figs. 6 and 7 demonstrate transmission of the structure of Fig. 5. The intensity of the incident light alters the nonlinear Kerr refractive index and this changes the total refractive index of Kerr medium. Consequently, the light resonant frequency of the cavity can shift. Ignoring the nonlinear properties of the defects ($N_2 = 0$), the resonant frequency of cavity can be shifted by changing the radii of the defects, as shown in Fig. 6.

By considering nonlinear properties of the defects, Fig. 7 shows that the light transmission is dependent on the light intensity at different wavelengths of $\lambda_1 = 1551, \lambda_2 = 1548, \lambda_3 = 1545$, and $\lambda_4 = 1542$ nm which are according to the radii of $r_{d1} = 0.22a$, $r_{d2} = 0.23a$, $r_{d3} = 0.24$, $r_{d4} = 0.25a$, respectively. Increasing the radii of nonlinear defects enhances their sensitivity to the incident light intensity which leads to the resonant frequency shift at low input light power. Also, the slope of transmission vs. input power becomes sharp by increasing the radii of defects. So, by adjusting the radii of defects and the radii of rods around defects, the sensitivity of the structure to different light intensity can be tuned in various designs and applications such as AOSDC.

3. The Novel AOADC

Fig. 8 shows the proposed AOADC having one input and two outputs A and B. Port B is set within a cavity where the light will be coupled into it, in the resonance condition. As it mentioned previously, the cavity is in resonance mode of a specific light intensity so, If the input light intensity is high, both outputs will turn to ON or equivalently logic “1”. Tuning the resonant frequency of the cavity for the input light, the light in output A will have three states of passing, blocking, and passing again by increasing the input light intensity, as shown in Fig. 8. It can be seen that by increasing the input power, the output power in ports A and B turn gradually from logic “00” to “11”. In Table 1, the input power and the associated logic levels are indicated for each output and Fig. 9 illustrates the variation of outputs powers vs input power value.

Figs. 10–13 show the simulated H_y accomplished b 2-D FDTD method. As it can be seen in the figure and table, if the input light

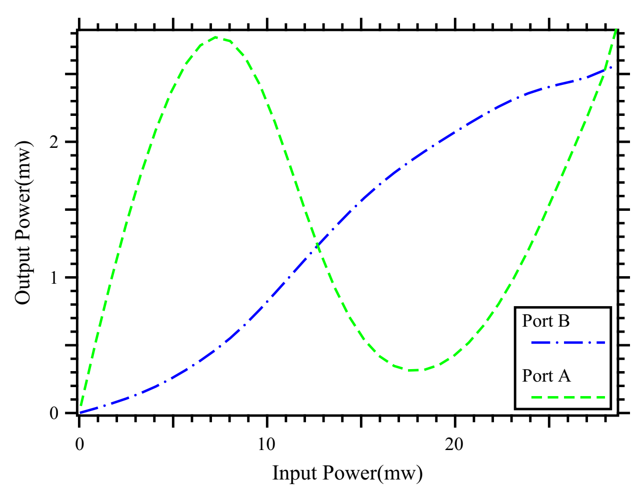

Fig. 9. Simulated output vs. input power for radii of $r_c = 0.33a$ and $r_d = 0.19a$ at $\lambda = 1550$ nm.

Table 1
Logic states level of proposed AOADC.

Input power	Output Port A	Output Port B	Logic
$0\text{ mW} < P_{in} < 2\text{ mW}$	$1.5\text{ mW} > P_A$	$0.02\text{ mW} > P_B$	“00”
$2\text{ mW} < P_{in} < 10\text{ mW}$	$1.5W < P_A < 2.9\text{ mW}$	$0.02\text{ mW} < P_B < 0.4\text{ mW}$	“01”
$10\text{ mW} < P_{in} < 25\text{ mW}$	$0.3\text{ mw} < P_A < 1.5\text{ mW}$	$1.2\text{ mW} < P_B < 2.4\text{ mW}$	“10”
$25\text{ mW} < P_{in}$	$1.5\text{ mW} < P_A$	$2.4\text{ mW} < P_B$	“11”

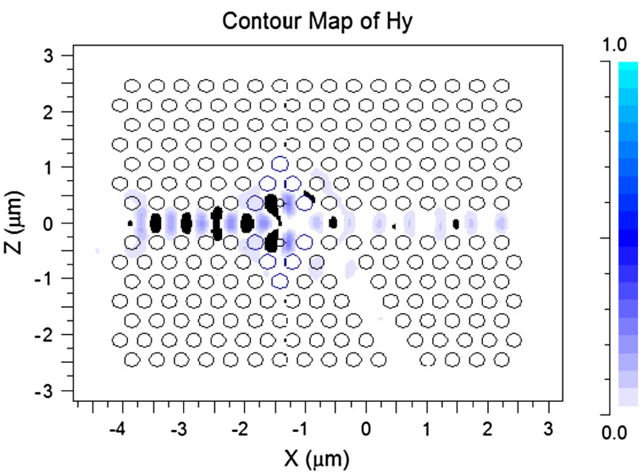

Fig. 10. H_y distribution for the designed ADC with the input power of 1.3 mW and output logic of “00”.

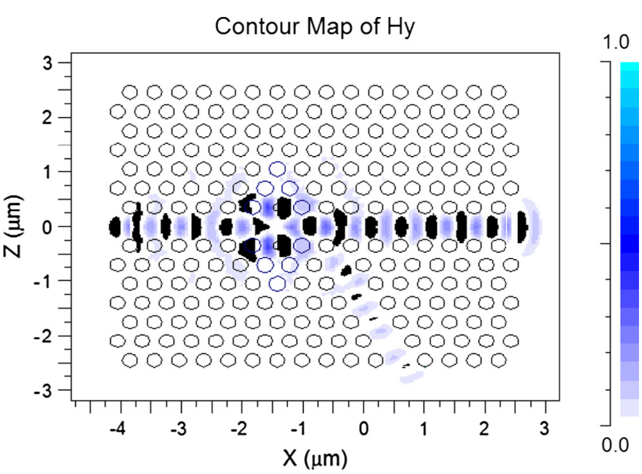

Fig. 11. H_y distribution for the designed ADC with the input power of 8 mW and output logic of “01”.

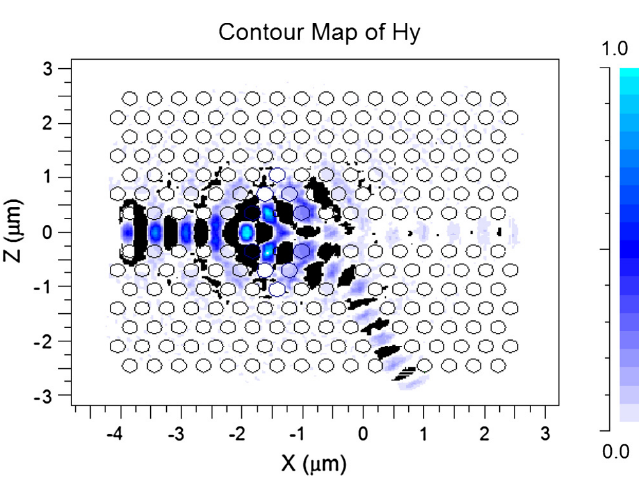

Fig. 12. H_y distribution for the designed ADC with the input power of 15 mW and output logic of “10”.

power is $0 < Pin < 2$ mW, the output of both ports A and B will be “0”, and if the input light power is $2\text{ mW} < Pin < 10$ mW, the output of ports B will be “0” and port A will be “1”. For the input light

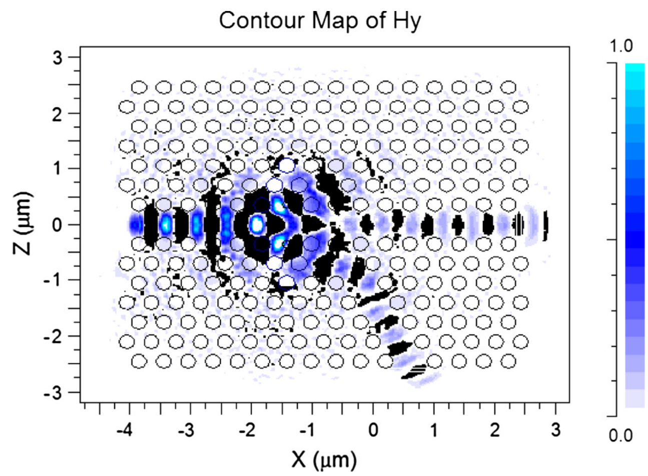

Fig. 13. H_y distribution for the designed ADC with the input power of 28 mW and output logic of “11”.

power of $10\text{ mW} < Pin < 25$ mW, the output of ports A and B will be “0” and “1”, respectively. Finally, if the input light power is $25\text{ mW} < Pin$, the frequency shift of cavity will occur again and the output of both ports will become “1”.

Here, The temporal shape of the input pulse is square pulse with 300 CT ($C = 3e^8$ m/s is the speed of light and T is time) length. By applying CW signal to the system the output state will be “10” and after 300 CT the source switches to OFF state. As Fig. 14 shows, the outputreaches the stable state after 100 CT, while it reaches to ON state in the 150 CT. So, the minimum time period for the input pulse should be more than 1 ps which results in a ADC with maximum sampling rate up to 1 TS/s. Due to using only one cavity which is very fast compared to the previously reported ADCs. In order to study of the structure response to the Gaussian source we applied 0.5 ps or 150 CT duration Gaussian signal to the system. It is obvious that the system cannot response to pulses with lower time duration (Fig. 15) The wavelength of laser source set to 1550 nm and wavelength of cavity resonance is 1540 nm. One of the important parameters in here is detuning between laser source frequency and cavity resonance frequency. This detuning governs the bistability manner of the structure. Based on Refs. [17,18], bistability appears when $\sigma > \sqrt{3}$ where $\sigma = (\omega_c - \omega_0)/\Gamma, Q = \omega_c/2\Gamma$, and Γ is the full width half minimum (FWHM). Here we obtained

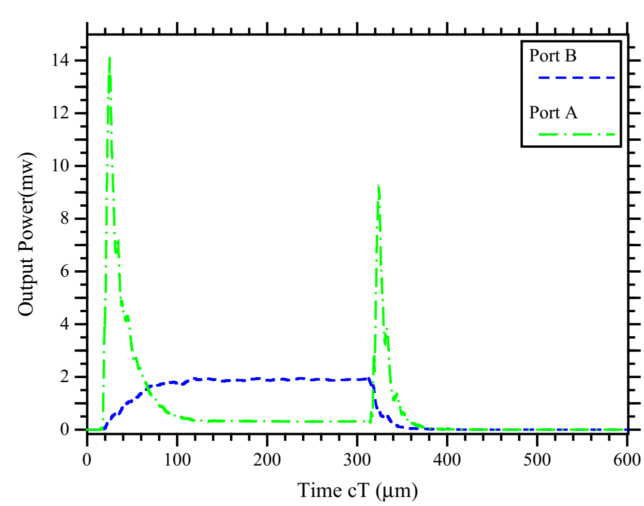

Fig. 14. The temporal diagram for the two outputs with input light interrupted at 300 CT µm.

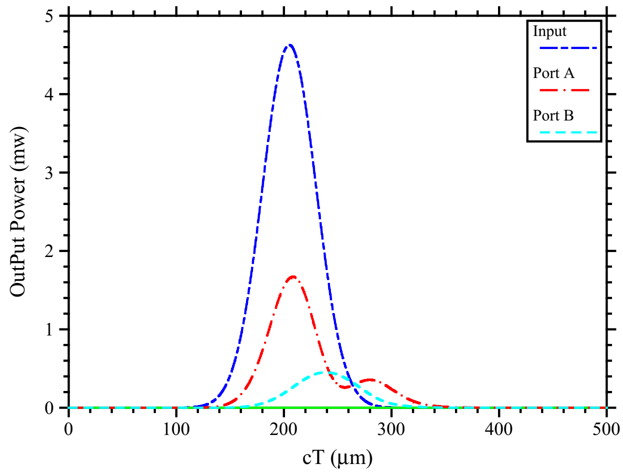

Fig. 15. Simulated output vs. input power for the radius of defect of 23a and radius of cavity rods of 0.32a.

Table 2
Energy reflection in the structure.

State of the operation	Reflected Power
"00"	0 mW < P_{ref} < 0.4 mW
"01"	0.4 mW < P_{ref} < 6 mW
"10"	6 mW < P_{ref} < 14 mW
"11"	14 mW < P_{ref} < 21 mW

$\sigma = 1.718$ and quality factor $Q = 71.591$ of cavity with resonant frequency $\omega_c = 0.65\ \mu m^{-}1$ and $\Delta\omega = (\omega_0 - \omega_c) = 0.005337\ \mu m^{-1}$ And so there is no bistability manner in the proposed structure. In the structure, at cavity resonance wavelength or $0.65\ \mu m^{-1}$ the amount of reflected energy to the input port is considerable where using this reflection provide possibility to increase the resolution of ADC, which results in adding extra output ports. Table 2 demonstrated energy reflection in the structure.

To adjust the ADC for higher power, the diameter of nonlinear defects can decrease which leads to the shorter resonant frequency. To adjust ADC to operate at 1550 nm and compensate the frequency shift due to change in the radii of nonlinear Kerr rods, the radii of the surrounding rods can increase, as discussed in the previous section. In this phase, the radii of nonlinear rods

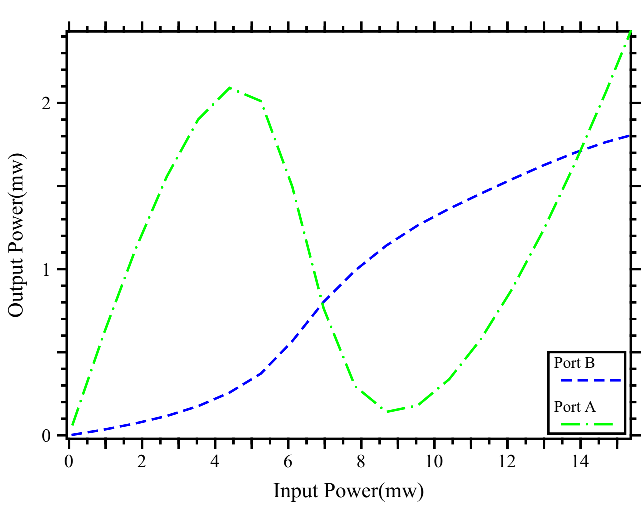

Fig. 16. Simulated output vs. input power for the radius of defect of 23a and radius of cavity rods of 0.32a.

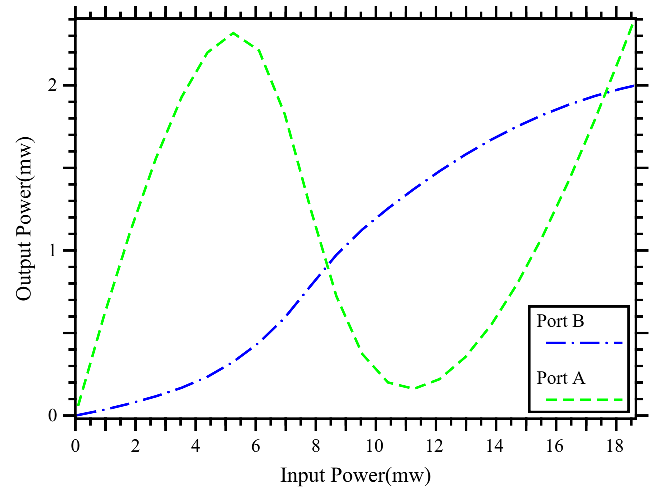

Fig. 17. Simulated output vs. input power for the radius of defect of 21a and radius of cavity rods of 0.322a.

Table 3
FDTD method parameters for simulation.

FDTD setup parameters	value
grid size	0.025 μm
Simulation time	1000 CT
Boundary conditions	PML
PML layers width	0.5 μm
Background index	1
Kerr nonlinearity	$2.7e^{-}9\ m^2/W^2$
time step	0.0125 CT

are set to 0.21a and 0.23a, and the radii of surrounding rods are set to 0.32a and 0.322a, and Figs. 16 and 17 show the simulation results. As it is can be seen in Figs. 14 and 15, the ADC is sensitive to the input power within the range of 0 to 13 mW and 0 to 18 mW, respectively. All of the simulations information and FDTD model parameters are listed in Table 3.

4. Conclusion

In this paper, a structure for AOADC was proposed and simulated. This two-bit AOADC has two output ports which change their state according to the input signal intensity. The designed AOADC operates in the range of communication wavelength (1550 nm). A cavity made of nonlinear Kerr material was used in this structure in order to obtain analog to digital conversion. Using nonlinear Kerr properties and PhC, the operation speed of the structure increased to 1 TS/s per second with the total footprint of 42 μm^2 which is a significant improvement comparing to the previously reported AOADCs. Employing 2-D FDTD method, the proposed structure was simulated for proof of principle.

References

[1] Y. Zhang, Y. Zhang, B. Li, Optical switches and logic gates based on self-collimated beams in two-dimensional photonic crystals, Opt. Express 15 (15) (2007) 9287–9292.
[2] T. Wang, Q. Li, D. Gao, Ultrafast polarization optical switch constructed from one-dimensional photonic crystal and its performance analysis, Chin. Sci. Bull. 54 (20) (2009) 3663.
[3] T. Nurmohammadi, K. Abbasian, R. Yadipour, M. As' adi, A novel proposal for or/nor logic gates based on dipole-induced transparency, Optik-Int. J. Light Electron Opt. 127 (18) (2016) 7115–7120.
[4] K. Goudarzi, A. Mir, I. Chaharmahali, D. Goudarzi, All-optical XOR and or logic gates based on line and point defects in 2-d photonic crystal, Opt. Laser Technol. 78 (2016) 139–142.

[5] Y.-C. Jiang, S.-B. Liu, H.-F. Zhang, X.-K. Kong, Realization of all optical half-adder based on self-collimated beams by two-dimensional photonic crystals, Opt. Commun. 348 (2015) 90–94.
[6] T. Nurmohammadi, K. Abbasian, M. Asadi, D. Jafari, Design of an ultrafast all-optical nor logic gate based on mach-zehnder interferometer using quantum-dot SOA, Optik-Int. J. Light Electron Opt. 125 (15) (2014) 4023–4029.
[7] M. Djavid, A. Ghaffari, F. Monifi, M.S. Abrishamian, T-shaped channel-drop filters using photonic crystal ring resonators, Physica E 40 (10) (2008) 3151–3154.
[8] M. Djavid, M. Abrishamian, Multi-channel drop filters using photonic crystal ring resonators, Optik-Int. J. Light Electron Opt. 123 (2) (2012) 167–170.
[9] A. Rostami, H.A. Banaei, F. Nazari, A. Bahrami, An ultra compact photonic crystal wavelength division demultiplexer using resonance cavities in a modified y-branch structure, Optik-Int. J. Light Electron Opt. 122 (16) (2011) 1481–1485.
[10] L. Jiu-Sheng, L. Han, Z. Le, Compact four-channel terahertz demultiplexer based on directional coupling photonic crystal, Opt. Commun. 350 (2015) 248–251.
[11] T. Nishitani, T. Konishi, K. Itoh, Resolution improvement of all-optical analog-to-digital conversion employing self-frequency shift and self-phase-modulation-induced spectral compression, IEEE J. Sel. Top. Quantum Electron. 14 (3) (2008) 724–732.
[12] T. Konishi, H. Goto, T. Kato, K. Kawanishi, All optical analog-to-digital conversion: principle and recent progress, in: 15th Asia-Pacific Conference on Communications, 2009. APCC 2009, IEEE, 2009, pp. 487–490.
[13] R. Pant, C. Xiong, S. Madden, B.L. Davies, B.J. Eggleton, Investigation of all-optical analog-to-digital quantization using a chalcogenide waveguide: a step towards on-chip analog-to-digital conversion, Opt. Commun. 283 (10) (2010) 2258–2262.
[14] B. Youssefi, M.K. Moravvej-Farshi, N. Granpayeh, Two bit all-optical analog-to-digital converter based on nonlinear kerr effect in 2d photonic crystals, Opt. Commun. 285 (13) (2012) 3228–3233.
[15] F. Mehdizadeh, M. Soroosh, H. Alipour-Banaei, E. Farshidi, All optical 2-bit analog to digital converter using photonic crystal based cavities, Opt. Quant. Electron. 49 (1) (2017) 38.
[16] M. Notomi, T. Tanabe, A. Shinya, E. Kuramochi, H. Taniyama, S. Mitsugi, M. Morita, Nonlinear and adiabatic control of high-q photonic crystal nanocavities, Opt. Express 15 (26) (2007) 17458–17481.
[17] H. Nakamura, Y. Sugimoto, K. Kanamoto, N. Ikeda, Y. Tanaka, Y. Nakamura, S. Ohkouchi, Y. Watanabe, K. Inoue, H. Ishikawa, et al., Ultra-fast photonic crystal/quantum dot all-optical switch for future photonic networks, Opt. Express 12 (26) (2004) 6606–6614.
[18] I. Fushman, D. Englund, A. Faraon, N. Stoltz, P. Petroff, J. Vučković, Controlled phase shifts with a single quantum dot, Science 320 (5877) (2008) 769–772.
[19] M. Danaie, H. Kaatuzian, Design and simulation of an all-optical photonic crystal and gate using nonlinear kerr effect, Opt. Quant. Electron. 44 (1-2) (2012) 27–34.
[20] M.F. Yanik, S. Fan, M. Soljačić, High-contrast all-optical bistable switching in photonic crystal microcavities, Appl. Phys. Lett. 83 (14) (2003) 2739–2741.
[21] Q. Li, T. Wang, Y. Su, M. Yan, M. Qiu, Coupled mode theory analysis of mode-splitting in coupled cavity system, Opt. Express 18 (8) (2010) 8367–8382.

Dariush Jafari received his MSc (Nano-photonic Engineering) in 2012 from the University of Tabriz. His research interests include plasmonics and photonic crystal based optical devices.

Tofiq Nurmohammadi received his MSc (Nano-electronics Engineering) in 2012 from the University of Tabriz. Now he is Ph.D. candidate at the University of Tabriz. His research interests include plasmonics and optics.

Javad Asadi received his MSc (Nano-photonic Engineering) in 2012 from the University of Tabriz. Now he is Ph.D. candidate at the Lehigh University. His research interests include nonlinear optics and nanophotonics.

Karim Abbasian received his Ph.D. (Electronic Engineering) in 2008 from the University of Tabriz. Now he is the associate professor at the school of engineering-emerging technologies in the University of Tabriz. His research interests also include photonics and optics.